

# Breast Histopathology Image Retrieval by Attention-based Adversarially Regularized Variational Graph Autoencoder with Contrastive Learning-Based Feature Extraction

Nematollah Saeidi<sup>a</sup>, Hossein Karshenas<sup>a,\*</sup>, Bijan Shoushtarian<sup>a,b</sup>, Sepideh Hatamikia<sup>c,d</sup>, Ramona Woitek<sup>c</sup>, Amirreza Mahbod<sup>c</sup>

<sup>a</sup>*Artificial Intelligence Department, Faculty of Computer Engineering, University of Isfahan, Isfahan, Iran*

<sup>b</sup>*Department of Computer Engineering Techniques, Mazaya University College, Nasiriyah, Iraq*

<sup>c</sup>*Research Center for Medical Image Analysis and Artificial Intelligence, Department of Medicine, Danube Private University, Krems an der Donau, Austria*

<sup>d</sup>*Austrian Center for Medical Innovation and Technology, Wiener Neustadt, Austria*

---

## Abstract

Breast cancer is a significant global health concern, particularly for women. Early detection and appropriate treatment are crucial in mitigating its impact, with histopathology examinations playing a vital role in swift diagnosis. However, these examinations often require a substantial workforce and experienced medical experts for proper recognition and cancer grading. Automated image retrieval systems have the potential to assist pathologists in identifying cancerous tissues, thereby accelerating the diagnostic process. Nevertheless, due to considerable variability among the tissue and cell patterns in histological images, proposing an accurate image retrieval model is very challenging.

This work introduces a novel attention-based adversarially regularized

---

\*Corresponding author

*Email addresses:* saeidi.n@eng.ui.ac.ir (Nematollah Saeidi), h.karshenas@eng.ui.ac.ir (Hossein Karshenas), shoushtarian@aim.com (Bijan Shoushtarian), sepideh.hatamikia@dp-uni.ac (Sepideh Hatamikia), ramona.woitek@dp-uni.ac.at (Ramona Woitek), amirreza.mahbod@dp-uni.ac.at (Amirreza Mahbod)

variational graph autoencoder model for breast histological image retrieval. Additionally, we incorporated cluster-guided contrastive learning as the graph feature extractor to boost the retrieval performance. We evaluated the proposed model’s performance on two publicly available datasets of breast cancer histological images and achieved superior or very competitive retrieval performance, with average mAP scores of 96.5% for the BreakHis dataset and 94.7% for the BACH dataset, and mVP scores of 91.9% and 91.3%, respectively.

Our proposed retrieval model has the potential to be used in clinical settings to enhance diagnostic performance and ultimately benefit patients.

*Keywords:* Computational pathology, Graph Neural Network, Graph Construction, Adversarial Training, Variational Graph Autoencoder, Attention Module, Image Retrieval

---

## 1. Introduction

Breast cancer is a significant health threat to women, leading to considerable mortality worldwide [1]. It is the most commonly diagnosed cancer worldwide and represents a quarter of all cancers diagnoses in women [2]. Female breast cancer mortality peaked in 1989 and has since decreased by 42% by 2021, translating to the avoidance of more than 490,000 deaths [3]. However, it is still one of the main causes of cancer death among women in recent years. For instance, according to 2018 statistics, breast cancer accounted for 15% of all cancer-related deaths and witnessed a 24% surge in new cases worldwide [4]. While breast cancer carries a high mortality rate, early detection and diagnosis followed by appropriate treatment can help mitigate its impact [5]. The urgency of early breast cancer detection has prompted innovative solutions, such as computer-aided diagnosis systems based on histological images [6]. This technology is a valuable tool to improve breast cancer diagnosis and ultimately can save lives [7]. However, proper diagnosis based on histological images often demands a substantial workforce and experienced medical experts. To overcome this challenge, pathologists can benefit from referring to archived databases for complex cases to find similar examples with verified findings to minimize diagnostic errors.

Content-based image retrieval (CBIR) is an approach to identify visually similar images in a database and can be used for various applications [8, 9]. For example, pathologists reviewing tissue sections for breast cancer diagno-

sis may benefit from searching through labeled histopathological image data for images resembling a case they are reviewing to improve their diagnostic accuracy in distinguishing cancerous from non-cancerous tissue. CBIR techniques have also been used for various non-medical applications such as "image search" for general and natural images, visual search for retail products, and multiple tools for recognizing faces and artworks [10]. Prior machine learning-based CBIR systems often employed models adapted to specific applications, requiring the collection of labeled data for each particular use, which presented a significant implementation challenge. Additionally, the notion of "similarity" in these approaches could have different interpretations depending on the specific context [11]. For instance, two histological images might be deemed similar because they originate from the same organ, depict the same type of cancer, share similar staining, or exhibit comparable histological characteristics.

Content-based medical image retrieval (CBMIR), a subset of CBIR, is specifically adapted to medical images and has been used in the context of radiology and histology in former studies [10, 11, 12]. CBMIR for histological images, not only aids histopathology in grading new tissue samples but also assists in analyzing patterns within similar tissues from previous patients [12, 6]. CBMIR offers distinct advantages over classification tasks. For instance, in classifying prostate cancer, a classification model provides class labels for each input. In contrast, a CBMIR system produces the top- $k$  most similar images based on a query image, where  $k$  represents the number of desired results. Upon availability, it can also provide other relevant information such as clinical meta-data or diagnosis reports [13]. Therefore, CBMIR provides pathologists and practitioners with more comprehensive information about diverse tissue patterns, enabling them to identify the most similar patterns within different tissues and minimize intra-and inter-observer variability [10, 14]. Another advantage of CBMIR is that it inherently includes a clinician-in-the-loop, which is often required for artificial intelligence (AI) applications in healthcare. Furthermore, a pathologist using CBMIR in the diagnostic process is required to come to their own diagnostic conclusion after incorporating additional information provided by CBMIR systems rather than replacing the pathologist's diagnosis with an AI-based classifier. Unlike histological images with their reports written by pathologists that are presented by CBMIR systems, a classifier is not necessarily easily interpretable and - even if presented to a clinician as a second opinion - may lead to automation bias [15, 16]. From a machine learning perspective, CB-

MIR is typically performed using unsupervised techniques, while classifiers are usually trained with supervised methods that require labeled datasets.

Histopathology image retrieval poses a significant challenge due to the substantial tissue and cell pattern variability [11]. Various semi- and fully-automatic approaches have been proposed for histopathology image retrieval [10]. Among these, graph neural networks (GNN) have gained considerable attention in recent years. Considering the grid data structure in images and the tremendous developments in convolutional neural networks (CNNs), many graph convolutional neural network (GCNN)-based architectures have also been extensively proposed for a wide range of computer vision tasks, including image retrieval [17]. In GCNN, input images can be represented as the graph nodes, and their features are usually extracted by pre-trained CNNs such as Visual Geometry Group (VGG) [18] or EfficientNet [19] to construct the graph. However, the exploited pre-trained models are typically trained on natural images, and their extracted features may not be optimally suited for medical data (e.g., histological images) [20, 21].

While GCNNs are usually trained in a supervised manner, some GCNN variants, such as variational graph autoencoder (VGAE) [22], can be used for unsupervised learning tasks. In VGAE, the encoder network maps input data to a lower-dimensional latent space, and the decoder network maps latent space vectors back to the original input data. Unlike conventional graph autoencoders (GAE), VGAE uses a probabilistic encoding function that maps input data to a probability distribution over the latent space. VGAE performance can be further enhanced by incorporating other techniques, such as adversarial training or adding an attention module to the model [22]. In adversarially regularized variational graph autoencoder (ARVGA) [23], the encoder is forced to generate embedding vectors closely resembling the data from a prior distribution through adversarial training. Incorporating an attention mechanism into CNNs [24] or GNNs [25] is another technique that has been exploited. These techniques have also been jointly applied for specific applications such as graph link prediction [26], graph clustering visualization [26], and node classification in partially labeled graphs [27].

In this study, for the first time, we adapted and exploited attention-based adversarially regularized variational graph autoencoders (A-ARVGAE) for the histological breast image retrieval task. Moreover, unlike previous studies that use conventional pre-trained CNNs for feature extraction to build the graph, we used the recently developed clustering-guided contrastive learning (CCL) feature extractor [28], which is explicitly designed for histopatholog-

ical images. We evaluated the performance of our proposed approach on two binary and multi-class histopathological breast image datasets, namely breast cancer histopathological database (BreakHis) [29] and breast cancer histology images dataset (BACH [30]), and achieved superior or very competitive performance compared to other state-of-the-art models. The main contribution of this research can be summarized as following:

- We adapted and exploited one of the state-of-the-art GNN models, which incorporated both attention mechanism and adversarial training for breast cancer histology image retrieval task.
- Instead of using conventional pre-trained CNNs as the node feature extractor, we made use of CLL, which is explicitly designed for histological images.
- Through extensive experiments, we show the effectiveness of our approach for both utilized GNN and feature extraction on two histopathological breast image datasets, namely BreakHis and BACH and achieved superior or very competitive performance compared to other approaches.

The rest of this paper is organized as follows: In Section 2, we present a background on methods for medical image retrieval and graph representation learning in histopathology. Section 3 describes our methodology, which contains all steps for the proposed framework. Section 4 consists of the experiments and evaluations with an analysis of the results. Finally, in Section 5, we conclude the paper with suggestions for future works.

## 2. Related Works

This section carries out a literature review for medical image retrieval and graph representation learning in histopathology, considering their relevance to our work.

### 2.1. Medical Image Retrieval

Various methods have been proposed in the literature for medical image retrieval. Text-based image retrieval systems were among the first attempts to find similar images in a given database. However, these methods rely heavily on expert annotation and proper keyword selection, making them generally considered ineffective and time-consuming [31].

CBMIR models, on the other hand, rely on the content (features) of the images instead of their given labels. Consequently, they can be used in an unsupervised manner without the need for manual labeling. Conventional CBMIR models consist of image preprocessing, hand-crafted or automatic feature extraction, and feature similarity measurements using different distance-based methods. To enhance interpretability, some approaches propose reducing the disparity between the extracted features and the high-level semantic meanings of the images by incorporating expert feedback or medical metadata into the retrieval model [31, 32].

Commonly used preprocessing methods include noise reduction, contrast enhancement, patch generation (e.g., from whole slide images), and normalization (e.g., stain normalization in histological images) [33, 34]. However, many novel machine learning (ML)- and deep learning (DL)-based feature extractors do not require any preprocessing steps. For feature extraction, both hand-crafted feature extractors and DL-based automatic feature extractors have been utilized. Hand-crafted features are employed to depict patches' morphological and textural characteristics. These features include color histogram-based features, histogram of oriented gradients (HOG) descriptor, local statistical features, global image structure tensor (GIST) features, Gabor features, wavelet-based features, intensity-based features, textural features, gray level co-occurrence matrix (GLCM) features, and scale-invariant feature transform (SIFT) descriptors [31, 28]. These features necessitate pre-defined transformation functions by experts. However, more recently, the rapidly evolving field of DL has streamlined the automatic high-level feature extraction process [11]. The ability of DL models to represent complicated patterns has made them a common approach for many image processing tasks.

Many pre-trained DL-based models, such as VGG19, ResNet, MobileNetV2, Xception, EfficientNet, and DenseNet121 have been used as feature extractors for tasks such as medical image classification or medical image retrieval [35, 36]. Hand-crafted or automatically extracted features of a query image are then compared to the image features in a database to find similar images. To do so, various similarity measurements such as distance-based retrieval (SDR), customized query approach (CQA), or nearest-neighbor matching can be used [37]. In the context of histopathology, Yottixel [38] and FISH [14] methods select the most distinctive patches to represent whole slide images (WSIs) through  $K$ -means clustering based on RGB histogram and spatial coordinate features. Yottixel employs a pre-trained DenseNet121,

trained on the ImageNet dataset [39], to extract patch embeddings, which are then transformed into binary barcodes. FISH trains a model based on an autoencoder on the cancer genome atlas (TCGA) dataset to encode an integer index for each patch during retrieval. However, it should be noted that using a pre-trained feature extractor (trained with natural images) alone may lead to suboptimal performance due to the domain shift between natural and histopathological images. A recent cutting-edge method introduces a pre-trained model, CCL [28], which is explicitly designed for histological images. CCL pretraining was conducted with around 15 million image patches extracted from more than 32,000 WSIs.

The CCL learning method leverages large-scale unlabeled histopathological image data, acquiring universal features that can be directly applied to subsequent WSI retrieval tasks. In our study, we utilized CCL as a robust and relevant feature extractor to build the graph.

## *2.2. Graph Representation Learning in Histopathology*

While CNNs have demonstrated impressive performance in medical image analysis, they often struggle to capture contextual information from neighboring areas, especially in scenarios with a limited field of view, such as patch-based analysis in histological images. In contrast to CNNs, GNNs excel at preserving complex correlations among neighboring elements during the learning process. GNNs have been successfully applied to various tasks, including tumor/object localization, classification, survival prediction, and image retrieval [40].

In the field of computational pathology, several GNN models, such as cell graphs, tissue graphs, cell-tissue graphs, and patch graphs, have been proposed for tasks like node classification (e.g., nuclei classification) or graph classification (e.g., histologic image patch categorization) [41, 42]. However, these applications have primarily been explored in a supervised manner and at times need sophisticated preprocessing, such as using other models like HoVerNet [43] or DDU-Net [44] to generate nuclei segmentation masks as input for the graph-based model. Concerning clinical applications, GNNs have found utility in different cancer types, including breast cancer, colorectal cancer, and prostate cancer, among others [42].

To construct a graph, one needs to define nodes, node embeddings, and edges. In the context of histological images, nodes could represent nuclei, image patches, or tissue regions. Node embeddings are features of the nodes that can be extracted either manually or automatically using pre-trained

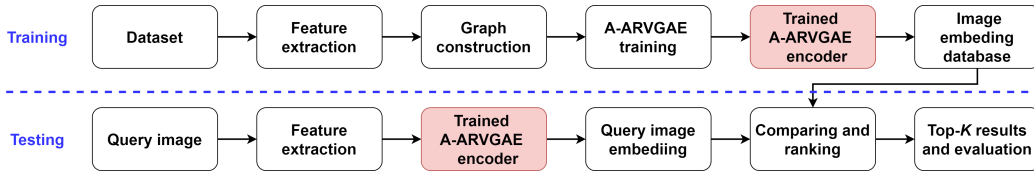


Figure 1: The general workflow of the proposed breast histological image retrieval model involves distinct processes for training and testing. A-ARVGAE: Attention-based adversarially regularized variational graph autoencoders.

models or other techniques. The edges depict connections between nodes, typically determined by predefined criteria such as  $k$ -nearest neighbors or distances between nodes. Once the graph is built, various GNN or GCN models can be applied, depending on the specific applications.

A GCN comprises several key components: an aggregation layer to define how features from neighbor nodes are aggregated, an activation layer to introduce non-linearity, graph pooling to reduce graph size (if needed), and graph convolutional operations to update node representations. It’s worth noting that other variants, such as GraphSAGE [45], GAT [46], or ChebNet [47] have been introduced in the literature as novel propagation rules to enhance performance across different applications. The output of a GNN typically depends on the application. For graph classification, a multilayer perceptron (MLP) can be employed atop the graph. In the case of graph reconstruction for unsupervised tasks, a linear projection decoder can be added to the model. As highlighted in a recent review [40], most GNN-based works in computational pathology are related to supervised classification tasks. Only a few studies have delved into histological image retrieval [40, 28, 48, 13]. However, even in these studies, the potential of attention mechanisms and adversarial training have not been explored. In our research, for the first time, we adapted and made use of both attention mechanism and adversarial training in variational graph autoencoders for the histological image retrieval task.

### 3. Methodology

The general workflow of our proposed approach for histological image retrieval is depicted in Figure 1. Subsequently, we discuss the details of the training process, followed by the application of the model in the testing phase for a given query image.



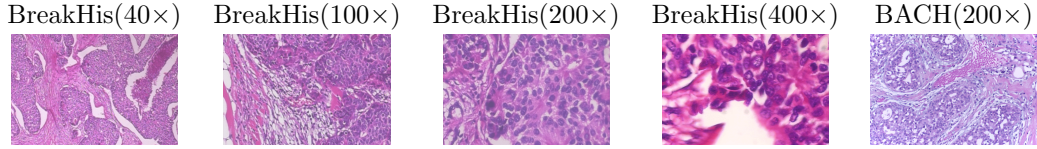


Figure 2: Example images from the BreakHis (first four images) and the BACH (last image) datasets.

### 3.1. Dataset

The dataset refers to a collection of histological image patches used to train and test the model. Each image has certain features and characteristics related to a specific class or histopathological grade. We use two breast histopathology image datasets in this study: BreakHis dataset [29] and BACH dataset [30], which are subsequently detailed. Example images from the datasets are shown in Figure 2.

- **BreakHis:** This dataset comprises hematoxylin and eosin (H&E)-stained breast histology microscopy images captured at various magnifications ( $40\times$ ,  $100\times$ ,  $200\times$ ,  $400\times$ ) and is categorized into two primary classes: benign and malignant classes. The dataset contains 7,909 images including 2,480 benign and 5,429 malignant samples with a size of  $700 \times 460$  pixels in Portable Network Graphics (PNG) format.
- **BACH:** This dataset comprises H&E-stained breast histology microscopy images captured at  $200\times$  magnification. It includes 400 images distributed across four distinct classes: benign (100 images), in situ carcinoma (100 images), invasive carcinoma (100 images), and normal (100 images), each with a resolution of  $2048 \times 1536$  pixels in Tagged Image File (TIF) format.

### 3.2. Feature Extraction

The first step in our proposed retrieval model is the extraction of features for all images in the dataset. Instead of using hand-crafted features or conventional pre-trained CNNs as feature extractors, we utilize CCL as the main feature extractor. Unlike other conventional pre-trained CNNs, CCL is trained with histological images. We hypothesize that using such a pre-trained feature extractor could lead to better descriptive features for the task of histological image retrieval.

We also use a set of standard baseline models as feature extractors and compare their retrieval performance with the CCL feature extractor. For this, we employ well-known pre-trained models, namely VGG19 [18], MobileNetV2 [49], DenseNet121 [50], Xception [51], InceptionResNetV2 [52], NASNetLarge [53], and EfficientNetV2M [19]. The details of these baseline pre-trained models are presented in Table 1. It is worth mentioning that all these pre-trained models are initially trained on natural images using the ImageNet dataset [39], but the CCL feature extractor used in this study is pre-trained with histological image patches. The results of these comparisons are reported in Section 4 (Table 2 and Table 3).

Table 1: Details of baseline feature extractors. All these pre-trained models are initially trained on natural images using the ImageNet dataset [39].

Feature Extraction Model	Size (MB)	Parameters	Depth
VGG19	549	143.7 M	19
MobileNetV2	14	3.5 M	105
DenseNet121	33	8.1 M	242
Xception	88	22.9 M	81
InceptionResNetV2	215	55.9 M	449
NASNetLarge	343	88.9 M	533
EfficientNetV2M	220	54.4 M	-

### 3.3. Graph Construction

GNNs are mostly applied on graph-based datasets. These datasets typically include nodes, node features, edges, and adjacency matrices. In contrast, non-structural datasets, such as those consisting of images, lack inherent graph structures. This makes graph construction a crucial step for applying GNNs to such data. For the retrieval task, graph construction methods often treat subjects (e.g., images) as graph nodes ( $V$ ), with the features of these subjects serving as node features ( $X$ ). Edges between nodes ( $E$ ) can be defined using distance metrics like cosine and Euclidean distances, indicating the likelihood of interaction between entities [54, 55, 56, 57]. The topology of these graphs is usually determined heuristically, employing strategies such as a pre-defined proximity threshold, a nearest neighbor rule, or a probabilistic model. To create edges between nodes, various algorithms such as  $k$  approximate nearest neighbor ( $k$ -ANN) can be used. In  $k$ -ANN, the exactness of the neighbor relationship is relaxed to gain efficiency. This approach is beneficial

in high-dimensional feature spaces, where the curse of dimensionality slows down exact nearest neighbor searches significantly. While there are various implementations of ANN algorithms, the ANN benchmark [58] is a widely-used library that encompasses most ANN-based methods. In our study, we utilize the fast library for approximate nearest neighbors (FLANN) to calculate distances between node embeddings, selecting the  $k$  nearest nodes to each entity as adjacent nodes. The computation of graph edges is conducted as follows:

$$e_{ij} = \begin{cases} 1 & \text{if } v_j \in k\text{-ANN}(v_i) \\ 0 & \text{otherwise} \end{cases} \quad (1)$$

where  $e_{ij} = 1$  indicates the existence of an edge connection between the  $i$ -th and  $j$ -th nodes in the graph, and  $e_{ij} = 0$  denotes no edge. Utilizing the edges and nodes, the adjacency matrix ( $A$ ) can be constructed where the values of the matrix ( $a_{ij}$ ) act as indicators, quantifying of the connections between nodes  $V_i$  and  $V_j$ .

It is worth mentioning that we use transductive learning, where the entire dataset (training, validation, and test data) is observed to build the graph. The summarized workflow to build the graph in our study is shown in Figure 3.

#### 3.4. A-ARVGAE

The overall architecture of the A-ARVGAE model is depicted in Figure 4. The proposed architecture comprises four main components: the encoder (yellow block), which also serves as the generator for adversarial training; the embedding latent space (pink block); the decoder (blue block); and the discriminator (green block), which is another essential component for adversarial training.

The constructed graph, as described in the previous section, is fed into the encoder of the A-ARVGAE model. The encoder includes a graph attention layer that performs attention operations, batch normalization, leaky ReLU, and dropout, followed by two graph convolutional layers. The attention-based convolutional operation integrating attention mechanisms into convolutional layers assigns varying weights to the neighbors, enabling the model to concentrate on the most relevant parts of the graph when learning node representations [46]. The attention mechanism aggregates information from adjacent nodes with an adaptive weight allocation to neighboring nodes. As

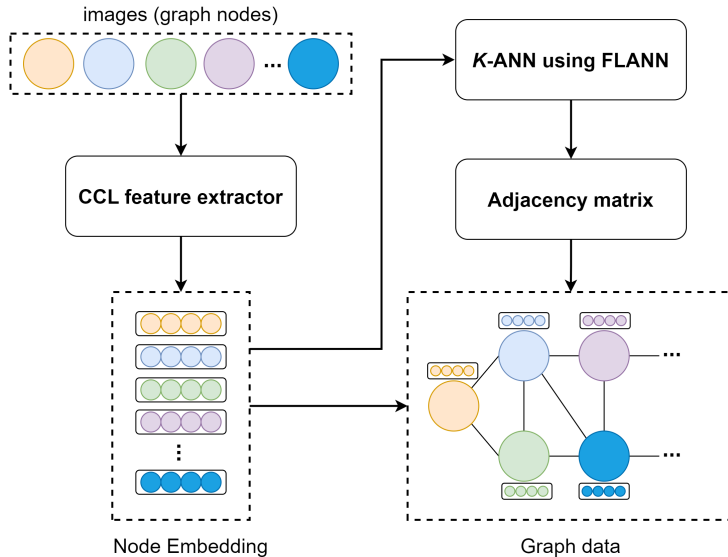


Figure 3: The framework of graph construction. CCL: Cluster guided contrastive learning,  $K$ -ANN:  $K$  approximate nearest neighbors, FLANN: fast library for approximate nearest neighbors

indicated by prior studies, the use of a multi-head attention layer has been shown to yield superior performance [26] and hence we also employ two-head attention layer in our work.

Inspired by the VGAE [20], the encoder in our architecture does not encode an input into a fixed latent representation. Instead, the outputs of the graph convolutional layers are parameters (mean ( $\mu$ ) and variance ( $\sigma$ )) that define a probability distribution over the possible latent representations, denoted as  $Z$ , characterized by a normal distribution  $N(\mu, \sigma)$ . Sampling from the latent space involves drawing samples from the distribution  $N(\mu, \sigma)$  to produce latent node embeddings. This process employs the reparameterization trick, as introduced in [20], which enables the backpropagation of gradients through the stochastic sampling process for gradient descent optimization.

The decoder block employs a linear projection through a straightforward inner product ( $Z * Z^T$ ) followed by a sigmoid function, which results in the reconstructed graph.

As the A-ARVGAE model incorporates adversarial training, it includes a generator and a discriminator. Within this framework, the encoder functions

analogously to a generator in an adversarial network [23]. The generator tries to deceive the discriminator by producing synthetic data, which, in this context, refers to latent variables generated from the encoding of graph data. On the other hand, the discriminator (green block) attempts to differentiate whether samples are derived from real data or the generator. The discriminator evaluates embeddings from the prior distribution (a Gaussian distribution) as real and those from the latent variable  $Z$  as synthetic or fake. The discriminator block comprises a straightforward MLP with two linear layers along with batch normalization, leaky reLU, and dropout to distinguish between real (a prior Gaussian distribution) and fake (latent space  $Z$ ) embeddings.

The complete model integrates three loss components: a regression-based reconstruction loss (related to VGAE), a Kullback–Leibler divergence loss (related to VGAE), and a binary cross-entropy loss (related to discriminator in adversarial training). Further details regarding the model architecture and cost functions can be found in the respective studies [23, 46].

We compare the results of our employed GNN model (A-ARVGAE) with other GNN-based models, namely GAE, VGAE, and ARVGA, and also with another non-GNN-based state-of-the-art approach, called RetCCL, represented in [28]. RetCCL is a model that is recently developed for the histological image retrieval task, which is based on CCL feature extraction and nearest neighbor search to find similar images in a given dataset. The results of these comparisons are reported in Section 4 (Table 4).

### 3.5. Trained Graph Encoder

After training, the trained A-ARVGAE encoder can transform any input image into a vector in the embedding space.

### 3.6. Image Embedding Database

The embeddings generated by the trained A-ARVGAE encoder in the previous step for each training image are stored in a database. This database is then utilized in the testing phase to identify the top- $K$  similar images for a given query image as explained in Section 3.7

### 3.7. Testing phase

As depicted in the lower part of Figure 1, for a query image, the model aims to identify the top  $K$  similar images in the database. Similar to the

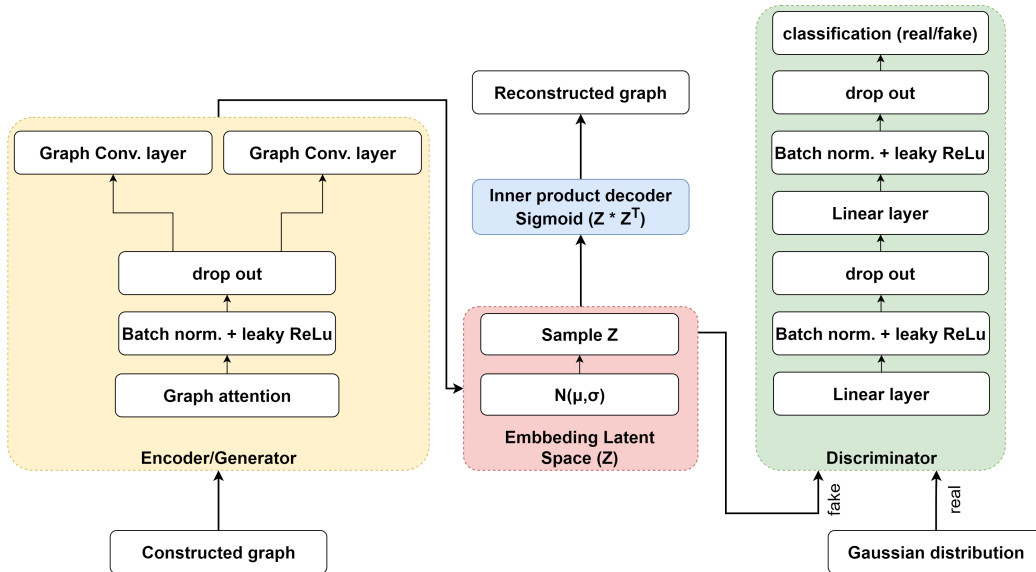


Figure 4: Architecture of attention-based adversarially regularized variational graph auto-encoder (A-ARVGAE). For interpretation of the references to color in this figure legend, the reader is referred to the web version of this article.

process with training images, features are first extracted from the test image using the CCL feature extractor. These features are then fed into the trained A-ARVGAE model to obtain the embedding in a lower-dimensional space, specifically from the encoder part of the model. After acquiring the embedding of the query image, it is compared with the embeddings in the image database to identify similar images. To find the most similar images, the ranking algorithm evaluates and ranks the candidate images based on Euclidean distance. These selected images are then arranged and ranked in ascending order according to Euclidean distances. Once ranked, the top- $K$  similar images are chosen as the final output of the retrieval model.

To evaluate the performance of the developed approach, we use two evaluation metrics, namely, mean Average Precision (mAP) [59] and mean Majority Vote (mMV) [14].

mAP is the average of the precision values computed at the ranks of relevant images in the retrieved results. It is a widely used metric for evaluating the effectiveness of a retrieval system. The formula for mAP is as follows:

$$mAP(k) = \frac{1}{|Q|} \sum_{q=1}^{|Q|} \frac{1}{|R_q|} \sum_{k=1}^{|R_q|} \text{Precision}(k) \cdot \text{rel}(k) \quad (17)$$

Where  $|Q|$  is the number of queries,  $R_q$  is the number of relevant images for query image  $q$ ,  $\text{Precision}(k)$  is the precision at rank  $k$  (the ratio of relevant images retrieved in the top  $k$  results to the total number of retrieved images up to rank  $k$ ),  $\text{rel}(k)$  is an indicator function that equals 1 if the image at rank  $k$  is relevant and 0 otherwise.  $|\cdot|$  denotes the length of the set.

mMV evaluates the frequency with which the primary diagnosis among the top- $k$  results aligns with the queried diagnosis as follows:

$$mMV(k) = \frac{1}{|Q|} \sum_{q=1}^{|Q|} 1\{L_q \in MV(\text{rel}(k))\} \quad (18)$$

Where  $L_q$  represents the ground truth diagnosis of the image, and MV is the predicted diagnosis of an image taken from the majority vote of top- $k$  samples. Similar to mAP,  $\text{rel}(k)$  is an indicator function that equals 1 if the image at rank  $k$  is relevant and 0 otherwise. Here,  $|\cdot|$  also denotes the length of the set.

## 4. Results & Discussion

In this section, we start with the implementation details, then delve into the experimental setup, and finally present the obtained results along with a detailed discussion.

### 4.1. Implementation Details

We used the PyTorch deep learning framework (version 2.2.0) and the PyTorch Geometric library (version 2.4.0) to implement the models. Adam optimizer was used to train the models with an initial learning rate (LR) of 0.0001. For dropout layers, a probability of 0.2 was chosen in the model architecture. All models were trained for 250 epochs, whereas in models with adversarial components, the discriminator was trained for five iterations in each epoch. To extract features from the training and test images, all images were down-sampled to  $256 \times 256$  pixels to fit into the utilized GPU memory. For each experiment, an identical training set (70%), validation set (10%), and test set (20%) were used to ensure fair comparisons between

different experiments. The data splitting was done randomly by keeping the ratio between different classes in the training, validation and test sets. In the process of graph construction, the parameter  $k$  was set to 25 for the BreakHis dataset and 15 for the BACH dataset. For the attention layer in the A-ARVGAE model, a 2-head attention layer was used. All experiments were conducted on a single machine using an NVIDIA GTX 1060 GPU and an Intel Core™ i7-9750H CPU.

#### 4.2. Experiments

We performed two sets of experiments for each dataset in this study.

In the first set, we investigated the effect of using the CCL feature extractor against other pre-trained models for the breast cancer histology image retrieval task. The results of this experiment for the BreakHis and BACH datasets are reported in Table 2 and Table 3, respectively. For a fair comparison, we used the A-ARVGAE model in all experiments.

As observed from Table 2 for the BreakHis dataset, the CCL feature extractor outperforms all other pre-trained feature extractor models across all metrics, except for 400× magnification, where DenseNet121 delivered better retrieval performance. However, for the average performance across all magnifications, CCL delivers the best results compared with all other pre-trained models, including DenseNet121. The results in Table 3 also indicate the superior performance of the CCL feature extractor compared with other pre-trained models for the BACH dataset.

Overall, the results reported in Table 2 and Table 3 for the BreakHis and BACH datasets show that the feature extractor trained on histological images outperforms feature extractors trained with non-medical images.

In the second experiment, we compare the performance of the employed A-ARVGAE model with other GNN-based and non-GNN-based models for both BreakHis and BACH datasets. The results of these experiments are presented in Table 4.

As shown in Table 4, the A-ARVGAE model surpasses all GNN-based models i.e., GAE, VGAE, and ARVGA for both datasets. The superior performance of the proposed model over ARVGA demonstrates the significance of the attention component in the employed architecture. An attention component allows the model to focus on specific parts of input data to calculate the model weights.

Compared with the RetCCL model, our approach delivers superior performance for both evaluation indices on the BACH dataset. However, for the



Table 2: Evaluation of the retrieval performance for the BreakHis dataset with different feature extractors. In all experiments attention-based adversarially regularized variational graph autoencoder is used as the retrieval model.

Magnification	Feature Extraction	mAP(5)	mMV(5)
40×	VGG19	0.945	0.859
	MobileNetV2	0.957	0.894
	DenseNet121	0.941	0.864
	Xception	0.899	0.743
	InceptionResNetV2	0.893	0.778
	NASNetLarge	0.925	0.809
	EfficientNetV2M	0.919	0.768
	CCL	<b>0.978</b>	<b>0.949</b>
100×	VGG19	0.948	0.850
	MobileNetV2	0.947	0.884
	DenseNet121	0.953	0.879
	Xception	0.903	0.739
	InceptionResNetV2	0.889	0.739
	NASNetLarge	0.919	0.777
	EfficientNetV2M	0.915	0.826
	CCL	<b>0.980</b>	<b>0.961</b>
200×	VGG19	0.941	0.840
	MobileNetV2	0.955	0.870
	DenseNet121	0.946	0.860
	Xception	0.904	0.796
	InceptionResNetV2	0.883	0.695
	NASNetLarge	0.921	0.776
	EfficientNetV2M	0.905	0.791
	CCL	<b>0.964</b>	<b>0.930</b>
400×	VGG19	0.945	0.861
	MobileNetV2	0.941	0.850
	DenseNet121	<b>0.955</b>	<b>0.895</b>
	Xception	0.911	0.784
	InceptionResNetV2	0.897	0.718
	NASNetLarge	0.906	0.751
	EfficientNetV2M	0.905	0.790
	CCL	0.940	0.839
BreakHis Avg.	VGG19	0.944	0.852
	MobileNetV2	0.950	0.874
	Xception	0.904	0.765
	InceptionResNetV2	0.890	0.727
	NASNetLarge	0.917	0.778
	EfficientNetV2M	0.911	0.791
	DenseNet121	0.948	0.874
	CCL	<b>0.965</b>	<b>0.919</b>

Table 3: Evaluation of the retrieval performance for the BACH dataset with different feature extractors. In all experiments attention-based adversarially regularized variational graph autoencoder is used as the retrieval model.

Magnification	Feature Extraction	mAP(5)	mMV(5)
200×	VGG19	0.899	0.787
	MobileNetV2	0.893	0.737
	DenseNet121	0.897	0.700
	Xception	0.887	0.687
	InceptionResNetV2	0.872	0.675
	NASNetLarge	0.892	0.800
	EfficientNetV2M	0.882	0.762
	CCL	<b>0.947</b>	<b>0.913</b>

BreakHis dataset, RetCLL shows slightly better performance for some magnifications. Nevertheless, our approach still yields superior results in other magnifications. The average results across all magnifications indicate the superior performance of our approach compared with RetCCL, based on the mAP(5) evaluation index (2.3% improved performance). However, for the MVP(5) score, RetCCL exhibits a better average performance with a 1.5% margin.

Overall, while our approach has demonstrated superior or very competitive performance in all experiments, it should be noted that GNN training typically requires large datasets [60]. The utilized model in this study was trained on the BreakHis and BACH datasets, which are relatively small.

For visual analysis, we randomly select five query images from the BreakHis and BACH test sets (four from the BreakHis with different magnifications and one from the BACH dataset) to visualize the model output (top five ranks). Figure 5 depicts the query images and model output. As the results show, the model is capable of providing relevant images (with identical classes as the query images) for most of the samples.

As suggested in [61], we also compare the embedding vectors of some example image pairs with different degrees of similarity in Figure 6. As shown in the figure, the embedding vectors for similar image pairs are very close to each other. In contrast, the embedding vectors for dissimilar pairs are separable.

Table 4: Comparison of different models (GNN-based models including GAE, VGAE, and ARVGA, non-GNN-based model, and ours) for the BreakHis and BACH datasets for the breast cancer histological image retrieval task. GAE: graph autoencoder, VGAE: variational graph autoencoder, ARVGA: adversarial regularized variational graph autoencoder, RetCCL: retrieval with cluster-guided contrastive learning

Dataset	Method	mAP(5)	mMV(5)
BreakHis (40×)	GAE	0.901	0.773
	VGAE	0.962	0.934
	ARVGA	0.969	0.909
	RetCCL	<b>0.983</b>	<b>0.9789</b>
	Ours	0.978	0.9499
BreakHis (100×)	GAE	0.910	0.792
	VGAE	0.966	0.903
	ARVGA	0.949	0.909
	RetCCL	0.970	0.951
	Ours	<b>0.980</b>	<b>0.961</b>
BreakHis (200×)	GAE	0.926	0.825
	VGAE	0.955	0.900
	ARVGA	0.949	0.879
	RetCCL	0.920	0.920
	Ours	<b>0.964</b>	<b>0.930</b>
BreakHis (400×)	GAE	0.924	0.828
	VGAE	0.923	0.806
	ARVGA	0.932	0.834
	RetCCL	0.897	<b>0.889</b>
	Ours	<b>0.940</b>	0.839
BreakHis Avg.	GAE	0.915	0.804
	VGAE	0.951	0.885
	ARVGA	0.949	0.882
	RetCCL	0.942	<b>0.934</b>
	Ours	<b>0.965</b>	0.919
BACH (200×)	GAE	0.919	0.740
	VGAE	0.937	0.798
	ARVGA	0.935	0.817
	RetCCL	0.901	0.8942
	Ours	<b>0.947</b>	<b>0.913</b>

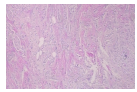
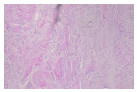
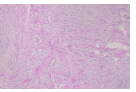
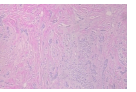
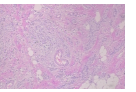
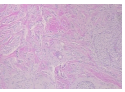
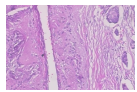
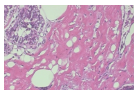
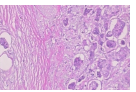
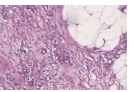
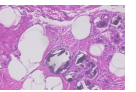
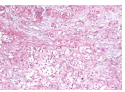
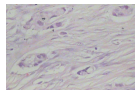
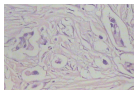
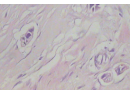
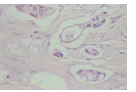
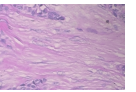
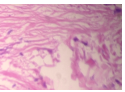
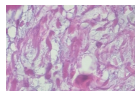
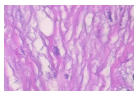
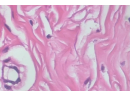
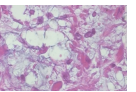
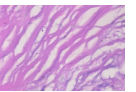
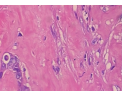
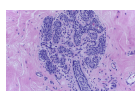
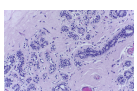
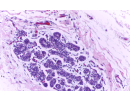
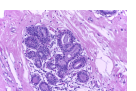
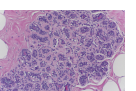
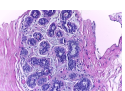
	Query	Rank 1	Rank 2	Rank 3	Rank 4	Rank 5
BH (40×)	 M	 M ✓	 M ✓	 M ✓	 M ✓	 M ✓
BH (100×)	 M	 BN ✗	 M ✓	 M ✓	 M ✓	 M ✓
BH (200×)	 M	 M ✓	 M ✓	 M ✓	 BN ✗	 BN ✗
BH (400×)	 M	 M ✓	 M ✓	 M ✓	 M ✓	 M ✓
BACH (200×)	 N	 N ✓	 N ✓	 N ✓	 N ✓	 N ✓

Figure 5: Five sample queries from the BreakHis and BACH datasets and their top similar retrieved images. Successful and unsuccessful retrieval are denoted by (✓) and (✗), respectively. M: Malignant class, BN: Benign class, N: Normal class, BH: BreakHis

## 5. Conclusion & Future Works

Recently, there has been a growing trend in utilizing GNNs to address challenges in analyzing histopathology images. This research introduces a new GNN-based approach specifically designed for breast histopathology image retrieval. We incorporated both attention mechanisms and adversarial training in a variational graph auto-encoder model to enhance retrieval performance. Moreover, instead of using conventional pre-trained models as the node feature extractor, we employed the CCL feature extractor, specifically

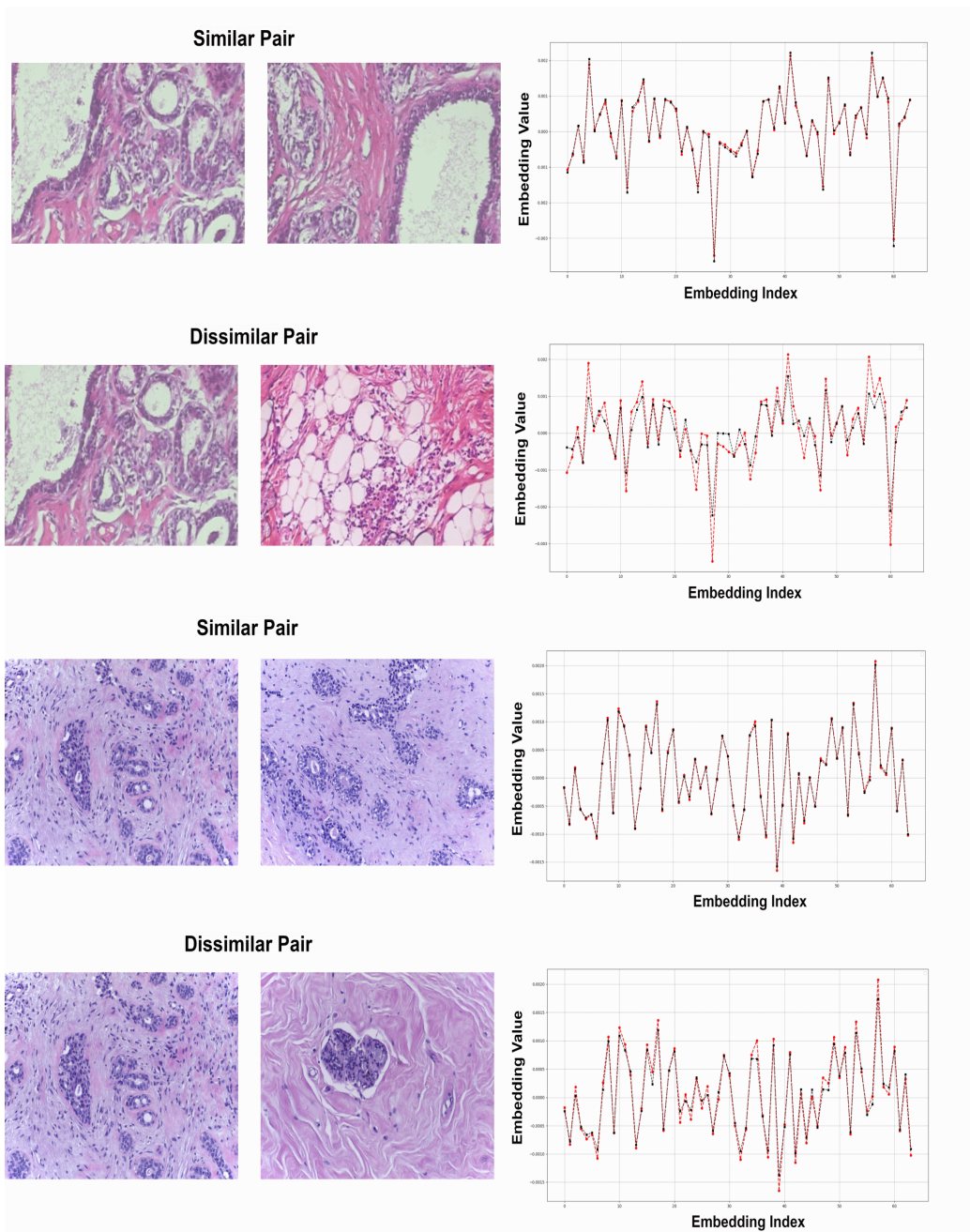


Figure 6: Comparison of embedding values for four image pairs. Similar pairs refer to images within the same class, and dissimilar pairs refer to images in different classes. The distances between the embedding of the two images in each image pair are shown on the right side of the figure. For each image pair, the left and right image embeddings are depicted in black and red, respectively.

pre-trained on histological images. Our results confirm that incorporating both attention mechanisms and adversarial training consistently exhibits superior performance compared to other GNN variants. Additionally, using the CCL feature extractor further boosts performance in our experiments. While our approach delivers promising results for breast histology image retrieval, certain aspects can be considered for further investigation in future studies.

Transformers-based models have shown impressive performance in various computer vision tasks. Some Transformer-based GNNs, such as graph transformer networks [62], have been developed for tasks such as node classification. Such models can be adapted and employed for the medical image retrieval task as well.

While we use FLANN to build the graph in our model, other state-of-the-art ANN methods and libraries, such as Faiss library [63] or HNSW method [9] can be exploited to enhance performance. However, it should be noted that most of these methods are slower in comparison to FLANN [37].

Another potential enhancement for the model is replacing the inner product decoder with a non-linear neural network, a topic that can be addressed in future studies.

Finally, using well-known boosting techniques, such as test-time augmentation or ensembling, has been shown to enhance performance for tasks such as medical image classification or segmentation [64, 65, 66]. Such techniques can also be incorporated into the workflow, and their impact on the retrieval performance can be investigated.

## **Acknowledgments**

This project is partially supported by the Ernst Mach Grant (reference number: MPC-2023-00569).

## **Conflict of Interest**

The authors declare that they have no known competing financial interests or personal relationships that could have appeared to influence the work reported in this paper.

## **Credit Authorship Contribution Statement**

Nematollah Saeidi: Conceptualization, Methodology, Investigation, Software, Writing – original draft. Hossein Karshenas: Supervision. Bijan

Shoushtarian: Supervision. Sepideh Hatamikia: Supervision. Ramona Woitek: Supervision. Amirreza Mahbod: Conceptualization, Validation, Review & editing, Supervision.

## References

- [1] R. Rashmi, K. Prasad, C. B. K. Udupa, Breast histopathological image analysis using image processing techniques for diagnostic puposes: A methodological review., *Journal of medical systems* 46 (1) (2021) 7. doi:<https://doi.org/10.1007/s10916-021-01786-9>.
- [2] M. Arnold, E. Morgan, H. Rungay, A. Mafra, D. Singh, M. Laver-sanne, J. Vignat, J. R. Gralow, F. Cardoso, S. Siesling, I. Soerjo-mataram, Current and future burden of breast cancer: Global statis-tics for 2020 and 2040, *The Breast* 66 (2022) 15–23. doi:<https://doi.org/10.1016/j.breast.2022.08.010>.
- [3] D. S. Dizon, A. H. Kamal, Cancer statistics 2024: All hands on deck, *CA: A Cancer Journal for Clinicians* 74 (1) (2024) 8–9. doi:<https://doi.org/10.3322/caac.21824>.
- [4] A. E. Minarno, K. M. Ghuftron, T. S. Sabrila, L. Husniah, F. D. S. Sumadi, CNN based autoencoder application in breast cancer im-age retrieval, in: *International Seminar on Intelligent Technology and Its Applications*, 2021, pp. 29–34. doi:<https://doi.org/10.1109/ISITIA52817.2021.9502205>.
- [5] H. Burstein, G. Curigliano, S. Loibl, P. Dubsy, M. Gnant, P. Poort-mans, M. Colleoni, C. Denkert, M. Piccart-Gebhart, M. Regan, H.-J. Senn, E. Winer, B. Thurlimann, Estimating the benefits of therapy for early-stage breast cancer: the st. gallen international consensus guide-lines for the primary therapy of early breast cancer 2019, *Annals of Oncology* 30 (10) (2019) 1541–1557. doi:<https://doi.org/10.1093/annonc/mdz235>.
- [6] Z. Tabatabaei, A. Colomer, K. Engan, J. Oliver, V. Naranjo, Resid-ual block convolutional auto encoder in content-based medical image retrieval, in: *IEEE 14th Image, Video, and Multidimensional Signal Processing Workshop*, 2022, pp. 1–5. doi:<https://doi.org/10.1109/IVMSP54334.2022.9816325>.

- [7] S. Fuster, F. Khoraminia, U. Kiraz, N. Kanwal, V. Kvikstad, T. Eftestøl, T. C. Zuiverloon, E. A. Janssen, K. Engan, Invasive cancerous area detection in non-muscle invasive bladder cancer whole slide images, in: IEEE 14th Image, Video, and Multidimensional Signal Processing Workshop, 2022, pp. 1–5. doi:<https://doi.org/10.1109/IVMSP54334.2022.9816352>.
- [8] D. Agrawal, A. Agarwal, D. K. Sharma, Content-based image retrieval (cbir): A review, in: P. K. Singh, Y. Singh, J. K. Chhabra, Z. Illés, C. Verma (Eds.), Recent Innovations in Computing, Springer Singapore, Singapore, 2022, pp. 439–452. doi:[https://doi.org/10.1007/978-981-16-8892-8\\_33](https://doi.org/10.1007/978-981-16-8892-8_33).
- [9] Y. A. Malkov, D. A. Yashunin, Efficient and robust approximate nearest neighbor search using hierarchical navigable small world graphs, IEEE Transactions on Pattern Analysis and Machine Intelligence 42 (4) (2020) 824–836. doi:<https://doi.org/10.1109/TPAMI.2018.2889473>.
- [10] L. Z, Z. X, M. H, Z. S, Large-scale retrieval for medical image analytics: A comprehensive review, Medical image analysis 43 (2018) 66–84. doi:<https://doi.org/10.1016/J.MEDIA.2017.09.007>.
- [11] N. Hegde, J. D. Hipp, Y. Liu, M. Emmert-Buck, E. Reif, D. Smilkov, M. Terry, C. J. Cai, M. B. Amin, C. H. Mermel, P. Q. Nelson, L. H. Peng, G. S. Corrado, M. C. Stumpe, Similar image search for histopathology: SMILY, npj Digital Medicine 2 (1) (2019). doi:<https://doi.org/10.1038/s41746-019-0131-z>.
- [12] J. Silva-Rodríguez, A. Colomer, M. A. Sales, R. Molina, V. Naranjo, Going deeper through the Gleason scoring scale: An automatic end-to-end system for histology prostate grading and cribriform pattern detection, Computer Methods and Programs in Biomedicine 195 (2020). doi:<https://doi.org/10.1016/j.cmpb.2020.105637>.
- [13] Y. Zheng, B. Jiang, J. Shi, H. Zhang, F. Xie, Encoding histopathological wsis using gnn for scalable diagnostically relevant regions retrieval, in: D. Shen, T. Liu, T. M. Peters, L. H. Staib, C. Essert, S. Zhou, P.-T. Yap, A. Khan (Eds.), Medical Image Computing and Computer Assisted Intervention, Springer International Publishing, Cham, 2019, pp. 550–558. doi:[https://doi.org/10.1007/978-3-030-32239-7\\_61](https://doi.org/10.1007/978-3-030-32239-7_61).



- [14] C. Chen, M. Y. Lu, D. F. Williamson, T. Y. Chen, A. J. Schaumberg, F. Mahmood, Fast and scalable search of whole-slide images via self-supervised deep learning, *Nature Biomedical Engineering* 6 (12) (2022). doi:<https://doi.org/10.1038/s41551-022-00929-8>.
- [15] S. Tang, A. Modi, M. Sjoding, J. Wiens, Clinician-in-the-loop decision making: Reinforcement learning with near-optimal set-valued policies, in: *International Conference on Machine Learning*, PMLR, 2020, pp. 9387–9396.
- [16] J. Herington, M. D. McCradden, K. Creel, R. Boellaard, E. C. Jones, A. K. Jha, A. Rahmin, P. J. Scott, J. J. Sunderland, R. L. Wahl, S. Zuehlsdorff, B. Saboury, Ethical considerations for artificial intelligence in medical imaging: Data collection, development, and evaluation, *Journal of Nuclear Medicine* 64 (12) (2023) 1848–1854. doi:<https://doi.org/10.2967/jnumed.123.266080>.
- [17] R. Yamashita, M. Nishio, R. K. G. Do, K. Togashi, Convolutional neural networks: an overview and application in radiology (2018). doi:<https://doi.org/10.1007/s13244-018-0639-9>.
- [18] K. Simonyan, A. Zisserman, Very deep convolutional networks for large-scale image recognition, *Computational and Biological Learning Society*, 2015, pp. 1–14.
- [19] M. Tan, Q. Le, EfficientNetV2: Smaller models and faster training, in: M. Meila, T. Zhang (Eds.), *Proceedings of the 38th International Conference on Machine Learning*, Vol. 139 of *Proceedings of Machine Learning Research*, PMLR, 2021, pp. 10096–10106.
- [20] T. N. Kipf, M. Welling, Variational graph auto-encoders, *arXiv preprint arXiv:1611.07308* (2016).
- [21] S. Denner, D. Zimmerer, D. Bounias, M. Bujotzek, S. Xiao, L. Kausch, P. Schader, T. Penzkofer, P. F. Jäger, K. Maier-Hein, Leveraging foundation models for content-based medical image retrieval in radiology, *arXiv preprint arXiv:2403.06567* (2024).
- [22] Z. Xiong, J. Cai, Multi-scale Graph Convolutional Networks with Self-Attention, *arXiv preprint arXiv:2112.03262* (2021).

- [23] S. Pan, R. Hu, G. Long, J. Jiang, L. Yao, C. Zhang, Adversarially regularized graph autoencoder for graph embedding, in: IJCAI International Joint Conference on Artificial Intelligence, Vol. 2018-July, 2018. doi:<https://doi.org/10.24963/ijcai.2018/362>.
- [24] M. Zheng, J. Xu, Y. Shen, C. Tian, J. Li, L. Fei, M. Zong, X. Liu, Attention-based CNNs for Image Classification: A Survey, in: Journal of Physics: Conference Series, Vol. 2171, 2022. doi:<https://doi.org/10.1088/1742-6596/2171/1/012068>.
- [25] H. Xia, S. Shao, C. Hu, R. Zhang, T. Qiu, F. Xiao, Robust clustering model based on attention mechanism and graph convolutional network, IEEE Transactions on Knowledge and Data Engineering 35 (5) (2023) 5203–5215. doi:<https://doi.org/10.1109/TKDE.2022.3150300>.
- [26] Z. Weng, W. Zhang, W. Dou, Adversarial Attention-Based Variational Graph Autoencoder, IEEE Access 8 (2020). doi:<https://doi.org/10.1109/ACCESS.2020.3018033>.
- [27] J. Xiao, Q. Dai, X. Xie, J. Lam, K. W. Kwok, Adversarially regularized graph attention networks for inductive learning on partially labeled graphs, Knowledge-Based Systems 268 (2023). doi:<https://doi.org/10.1016/j.knosys.2023.110456>.
- [28] X. Wang, Y. Du, S. Yang, J. Zhang, M. Wang, J. Zhang, W. Yang, J. Huang, X. Han, RetCCL: Clustering-guided contrastive learning for whole-slide image retrieval, Medical Image Analysis 83 (2023). doi:<https://doi.org/10.1016/j.media.2022.102645>.
- [29] F. A. Spanhol, L. S. Oliveira, C. Petitjean, L. Heutte, A Dataset for Breast Cancer Histopathological Image Classification, IEEE Transactions on Biomedical Engineering 63 (7) (2016). doi:<https://doi.org/10.1109/TBME.2015.2496264>.
- [30] G. Aresta, T. Araújo, S. Kwok, S. S. Chennamsetty, M. Safwan, V. Alex, B. Marami, M. Prastawa, M. Chan, M. Donovan, G. Fernandez, J. Zeineh, M. Kohl, C. Walz, F. Ludwig, S. Braunewell, M. Baust, Q. D. Vu, M. N. N. To, E. Kim, J. T. Kwak, S. Galal, V. Sanchez-Freire, N. Brancati, M. Frucci, D. Riccio, Y. Wang, L. Sun, K. Ma, J. Fang, I. Kone, L. Boulmane, A. Campilho, C. Eloy, A. Polónia, P. Aguiar,

- BACH: Grand challenge on breast cancer histology images, *Medical Image Analysis* 56 (2019). doi:<https://doi.org/10.1016/j.media.2019.05.010>.
- [31] R. Vishraj, S. Gupta, S. Singh, A comprehensive review of content-based image retrieval systems using deep learning and hand-crafted features in medical imaging: Research challenges and future directions, *Computers and Electrical Engineering* 104 (2022). doi:<https://doi.org/10.1016/j.compeleceng.2022.108450>.
- [32] S. Graham, F. Minhas, M. Bilal, M. Ali, Y. W. Tsang, M. Eastwood, N. Wahab, M. Jahanifar, E. Hero, K. Dodd, H. Sahota, S. Wu, W. Lu, A. Azam, K. Benes, M. Nimir, K. Hewitt, A. Bhalerao, A. Robinson, H. Eldaly, S. E. Raza, K. Gopalakrishnan, D. Snead, N. Rajpoot, Screening of normal endoscopic large bowel biopsies with interpretable graph learning: A retrospective study, *Gut* 72 (9) (2023). doi:<https://doi.org/10.1136/gutjnl-2023-329512>.
- [33] N. T. Singh, C. Kaur, A. Chaudhary, S. Goyal, Preprocessing of medical images using deep learning: A comprehensive review, in: *International Conference on Augmented Intelligence and Sustainable Systems, 2023*, pp. 521–527. doi:<https://doi.org/10.1109/ICAISS58487.2023.10250462>.
- [34] D. Murcia-Gómez, I. Rojas-Valenzuela, O. Valenzuela, Impact of image preprocessing methods and deep learning models for classifying histopathological breast cancer images, *Applied Sciences* 12 (22) (2022). doi:<https://doi.org/10.3390/app122211375>.
- [35] C. C. Ukwuoma, M. A. Hossain, J. K. Jackson, G. U. Nneji, H. N. Monday, Z. Qin, Multi-Classification of Breast Cancer Lesions in Histopathological Images Using DEEP\_Pachi: Multiple Self-Attention Head, *Diagnostics* 12 (5) (2022). doi:<https://doi.org/10.3390/diagnostics12051152>.
- [36] A. Mahbod, G. Schaefer, R. Ecker, I. Ellinger, Pollen grain microscopic image classification using an ensemble of fine-tuned deep convolutional neural networks, in: *International Conference on Pattern Recognition, Springer, 2021*, pp. 344–356. doi:[https://doi.org/10.1007/978-3-030-68763-2\\_26](https://doi.org/10.1007/978-3-030-68763-2_26).

- [37] D. A. Suju, H. Jose, FLANN: Fast approximate nearest neighbour search algorithm for elucidating human-wildlife conflicts in forest areas, in: 2017 4th International Conference on Signal Processing, Communication and Networking, ICSCN 2017, 2017. doi:<https://doi.org/10.1109/ICSCN.2017.8085676>.
- [38] S. Kalra, H. R. Tizhoosh, C. Choi, S. Shah, P. Diamandis, C. J. Campbell, L. Pantanowitz, Yottixel – An Image Search Engine for Large Archives of Histopathology Whole Slide Images, *Medical Image Analysis* 65 (2020) 101757. doi:<https://doi.org/10.1016/J.MEDIA.2020.101757>.
- [39] J. Deng, W. Dong, R. Socher, L.-J. Li, K. Li, L. Fei-Fei, ImageNet: A large-scale hierarchical image database, in: *IEEE Conference on Computer Vision and Pattern Recognition*, 2009, pp. 248–255. doi:<https://doi.org/10.1109/CVPR.2009.5206848>.
- [40] D. Ahmedt-Aristizabal, M. A. Armin, S. Denman, C. Fookes, L. Petersson, Graph-based deep learning for medical diagnosis and analysis: Past, present and future, *Sensors* 21 (14) (2021). doi:<https://doi.org/10.3390/s21144758>.
- [41] D. Anand, S. Gadiya, A. Sethi, Histograms: graphs in histopathology, in: J. E. Tomaszewski, A. D. Ward (Eds.), *Medical Imaging 2020: Digital Pathology*, Vol. 11320, SPIE, 2020, p. 113200O. doi:<https://doi.org/10.1117/12.2550114>.
- [42] D. Ahmedt-Aristizabal, M. A. Armin, S. Denman, C. Fookes, L. Petersson, A survey on graph-based deep learning for computational histopathology, *Computerized Medical Imaging and Graphics* 95 (2022) 102027. doi:<https://doi.org/10.1016/j.compmedimag.2021.102027>.
- [43] S. Graham, Q. D. Vu, S. E. A. Raza, A. Azam, Y. W. Tsang, J. T. Kwak, N. Rajpoot, Hover-Net: Simultaneous segmentation and classification of nuclei in multi-tissue histology images, *Medical Image Analysis* 58 (2019) 101563. doi:<https://doi.org/10.1016/j.media.2019.101563>.

- [44] A. Mahbod, G. Schaefer, G. Dorffner, S. Hatamikia, R. Ecker, I. Ellinger, A dual decoder u-net-based model for nuclei instance segmentation in hematoxylin and eosin-stained histological images, *Frontiers in Medicine* 9 (2022). doi:<https://doi.org/10.3389/fmed.2022.978146>.
- [45] W. Hamilton, Z. Ying, J. Leskovec, Inductive representation learning on large graphs, *Advances in neural information processing systems* 30 (2017).
- [46] P. Veličković, G. Cucurull, A. Casanova, A. Romero, P. Lio, Y. Bengio, Graph attention networks, *arXiv preprint arXiv:1710.10903* (2017).
- [47] H. Sahbi, Learning laplacians in chebyshev graph convolutional networks, in: *Proceedings of the IEEE/CVF International Conference on Computer Vision*, 2021, pp. 2064–2075.
- [48] Y. Zheng, Z. Jiang, H. Zhang, F. Xie, Y. Ma, H. Shi, Y. Zhao, Histopathological Whole Slide Image Analysis Using Context-Based CBIR, *IEEE Transactions on Medical Imaging* 37 (7) (2018). doi:<https://doi.org/10.1109/TMI.2018.2796130>.
- [49] M. Sandler, A. Howard, M. Zhu, A. Zhmoginov, L.-C. Chen, MobileNetV2: Inverted residuals and linear bottlenecks, in: *Proceedings of the IEEE Conference on Computer Vision and Pattern Recognition*, 2018. doi:<https://doi.org/10.1109/CVPR.2018.00474>.
- [50] G. Huang, Z. Liu, L. Van Der Maaten, K. Q. Weinberger, Densely connected convolutional networks, in: *IEEE Conference on Computer Vision and Pattern Recognition*, 2017, pp. 2261–2269. doi:<https://doi.org/10.1109/CVPR.2017.243>.
- [51] F. Chollet, Xception: Deep learning with depthwise separable convolutions, in: *IEEE Conference on Computer Vision and Pattern Recognition*, 2017, pp. 1800–1807. doi:<https://doi.org/10.1109/CVPR.2017.195>.
- [52] C. Szegedy, V. Vanhoucke, S. Ioffe, J. Shlens, Z. Wojna, Rethinking the inception architecture for computer vision, in: *IEEE Conference on Computer Vision and Pattern Recognition*, 2016, pp. 2818–2826. doi:<https://doi.org/10.1109/CVPR.2016.308>.

- [53] B. Zoph, V. Vasudevan, J. Shlens, Q. V. Le, Learning transferable architectures for scalable image recognition, in: IEEE/CVF Conference on Computer Vision and Pattern Recognition, 2018, pp. 8697–8710. doi:<https://doi.org/10.1109/CVPR.2018.00907>.
- [54] M. Adnan, S. Kalra, H. R. Tizhoosh, Representation Learning of Histopathology Images using Graph Neural Networks, IEEE Computer Society Conference on Computer Vision and Pattern Recognition Workshops 2020-June (2020) 4254–4261. arXiv:2004.07399, doi:<https://doi.org/10.1109/CVPRW50498.2020.00502>.
- [55] M. Lin, K. Wen, X. Zhu, H. Zhao, X. Sun, Graph Autoencoder with Preserving Node Attribute Similarity, Entropy 25 (4) (2023). doi:<https://doi.org/10.3390/e25040567>.
- [56] Y. Zheng, Z. Jiang, F. Xie, J. Shi, H. Zhang, J. Huai, M. Cao, X. Yang, Diagnostic Regions Attention Network (DRA-Net) for Histopathology WSI Recommendation and Retrieval, IEEE Transactions on Medical Imaging 40 (3) (2021). doi:<https://doi.org/10.1109/TMI.2020.3046636>.
- [57] Z. Gao, Z. Lu, J. Wang, S. Ying, J. Shi, A Convolutional Neural Network and Graph Convolutional Network Based Framework for Classification of Breast Histopathological Images, IEEE Journal of Biomedical and Health Informatics 26 (7) (2022). doi:<https://doi.org/10.1109/JBHI.2022.3153671>.
- [58] M. Aumüller, E. Bernhardsson, A. Faithfull, Ann-benchmarks: A benchmarking tool for approximate nearest neighbor algorithms, in: Similarity Search and Applications: 10th International Conference, SISAP 2017, Munich, Germany, October 4-6, 2017, Proceedings 10, Springer, 2017, pp. 34–49.
- [59] Y. Zheng, Z. Jiang, J. Shi, F. Xie, H. Zhang, W. Luo, D. Hu, S. Sun, Z. Jiang, C. Xue, Encoding histopathology whole slide images with location-aware graphs for diagnostically relevant regions retrieval, Medical Image Analysis 76 (2022). doi:<https://doi.org/10.1016/j.media.2021.102308>.

- [60] Z. Wu, S. Pan, F. Chen, G. Long, C. Zhang, P. S. Yu, A comprehensive survey on graph neural networks, *IEEE Transactions on Neural Networks and Learning Systems* 32 (1) (2021). doi:<https://doi.org/10.1109/tnnls.2020.2978386>.
- [61] E. Parcham, M. Ilbeygi, M. Amini, CBCapsNet: A novel writer-independent offline signature verification model using a cnn-based architecture and capsule neural networks, *Expert Systems with Applications* 185 (2021) 115649. doi:<https://doi.org/10.1016/j.eswa.2021.115649>.
- [62] S. Yun, M. Jeong, S. Yoo, S. Lee, S. S. Yi, R. Kim, J. Kang, H. J. Kim, Graph transformer networks: Learning meta-path graphs to improve gnn, *Neural Networks* 153 (2022) 104–119. doi:<https://doi.org/10.1016/j.neunet.2022.05.026>.
- [63] J. Johnson, M. Douze, H. Jégou, Billion-scale similarity search with GPUs, *IEEE Transactions on Big Data* 7 (3) (2021) 535–547. doi:<https://doi.org/10.1109/TBDATA.2019.2921572>.
- [64] N. Moshkov, B. Mathe, A. Kertesz-Farkas, R. Hollandi, P. Horvath, Test-time augmentation for deep learning-based cell segmentation on microscopy images, *Scientific Reports* 10 (1) (2020) 1–7. doi:<https://doi.org/10.1038/s41598-020-61808-3>.
- [65] A. Mahbod, G. Dorffner, I. Ellinger, R. Woitek, S. Hatamikia, Improving generalization capability of deep learning-based nuclei instance segmentation by non-deterministic train time and deterministic test time stain normalization, *Computational and Structural Biotechnology Journal* 23 (2024) 669–678. doi:<https://doi.org/10.1016/j.csbj.2023.12.042>.
- [66] B. Bancher, A. Mahbod, I. Ellinger, R. Ecker, G. Dorffner, Improving mask r-cnn for nuclei instance segmentation in hematoxylin & eosin-stained histological images, in: *MICCAI Workshop on Computational Pathology*, Vol. 156, 2021, pp. 20–35.